Energy-Resolved Information Scrambling in Energy-Space Lattices

S. Pegahan, I. Arakelyan, and J. E. Thomas.

*
Department of Physics, North Carolina State University, Raleigh, North Carolina 27695, USA

(

(Received 4 September 2020; revised 10 December 2020; accepted 28 January 2021; published 19 February 2021)

Weakly interacting Fermi gases simulate spin lattices in energy space, offering a rich platform for investigating information spreading and spin coherence in a large many-body quantum system. We show that the collective spin vector can be determined as a function of energy from the measured spin density, enabling general energy-space resolved protocols. We measure an out-of-time-order correlation function in this system and observe the energy dependence of the many-body coherence.

DOI: 10.1103/PhysRevLett.126.070601

Trapped, weakly interacting Fermi gases provide a new paradigm for the study of many-body physics in a large quantum system containing $N \simeq 10^5$ atoms with a tunable, reversible Hamiltonian [1,2]. In this system, coherent superpositions of two hyperfine states behave as pseudospins and the s-wave scattering length is magnetically tuned to nearly vanish [1,3,4]. The corresponding collision rate is negligible, so that single atom energies are conserved [1,5–7] over the experimental timescale. The conserved single particle energy states label the "sites" of an effective energy-space lattice, simulating a variety of spin-lattice models [8]. Interactions are effectively long range in energy space [4,8,9], important for new studies of information scrambling in a far from equilibrium, nearly zero temperature regime [10] and for applications to fast scrambling [11] and "out-of-equilibrium" dynamics in spin-lattice systems [12]. However, measurements in weakly interacting Fermi gases [1–7] have been limited to the spatial profiles of the collective spin density or the total number of atoms in each spin state, precluding observation of manybody correlations in chosen sectors of the energy-space lattice.

Of particular interest is the measurement of out-of-timeorder correlation (OTOC) functions in weakly interacting Fermi gases. Certain OTOC functions [13–16] can serve as entanglement witnesses and to quantify coherence and information scrambling in quantum many-body systems [10,17]. Originally, OTOC measurements were performed by reversing the time evolution of the many-body state in nuclear magnetic resonance experiments at high temperatures, where the initial state is described by a density operator and high order quantum coherence was observed [18]. New OTOC studies have been done in trapped ion systems containing relatively small numbers of atoms, where the individual sites are nearly equivalent, and the initial state is pure [10]. Related methods have been developed for systems containing up to 100 atoms [19]. but the application of OTOC measurement to trapped ultracold gases has remained a challenge.

In this Letter, we report the demonstration of a general method for performing energy-resolved measurements of the collective spin vector in a harmonically trapped weakly interacting Fermi gas. We show that OTOC measurements can be implemented in this system and we extract many-body coherence in energy-resolved sectors, paving the way for new protocols, such as time-dependent energy-space correlation measurements.

In the experiments [20], we begin with a degenerate cloud of 6 Li containing a total of $N=6.5\times 10^4$ atoms in a single spin state. The cloud is confined in a harmonic, cigar-shaped optical trap, with oscillation frequencies $\omega_x/2\pi=23$ Hz along the cigar x axis and $\omega_r/2\pi=625$ Hz in the transverse (y,z) directions. The corresponding Fermi temperature $T_F=0.73~\mu{\rm K}$ and $T/T_F=0.32$.

We employ the two lowest hyperfine-Zeeman states, which are denoted by $|1\rangle \equiv |\uparrow_z\rangle$ and $|2\rangle \equiv |\downarrow_z\rangle$. The cloud is initially prepared in state $|\downarrow_z\rangle$ in a bias magnetic field of 528.53 G, where the *s*-wave scattering length $a_{12} \equiv a = 4.24a_0$ [4]. In this case, the largest possible collision rate γ_c in the Fermi gas arises for an incoherent mixture with N/2 atoms in each of two spin states. We find $\gamma_c < 1.7 \times 10^{-3} \text{ s}^{-1}$ [21], which is negligible for the experimental timescale < 1 s. Hence, the single particle energies are conserved and the energy distribution is time independent, as observed in the experiments [4,20].

The Hamiltonian for the confined weakly interacting Fermi gas can be approximated as a one-dimensional (1D) spin "lattice" in energy space [4],

$$H(a) = a \sum_{i,j \neq i} g_{ij} \mathbf{s}_i \cdot \mathbf{s}_j - \sum_i \Omega_i s_{zi}, \tag{1}$$

where we take $\hbar \equiv 1$. We associate a "site" i with the energy $E_i = (n_i + 1/2)h\nu_x$ of an atom in the ith harmonic oscillator state along the cigar axis x. For each E_i , we define a dimensionless collective spin vector $\mathbf{s}_i = \sum_{\alpha_i} \mathbf{s}_{\alpha_i}$, where the sum over α_i includes the occupied transverse (n_y, n_z)

states for fixed n_i . As $k_B T_F / \hbar \omega_x \simeq 650$, the average number of atoms at each site is $N/650 \simeq 100$ [22].

The first term in Eq. (1) is a site-to-site interaction, proportional to the s-wave scattering length a and to the overlap of the harmonic oscillator probability densities for colliding atoms, $g_{ij} \propto \int dx |\phi_{E_i}(x)|^2 |\phi_{E_j}(x)|^2 \propto 1/\sqrt{|E_i-E_j|}$, which is an effective long-range interaction in the energy lattice [4]. For a zero temperature Fermi gas, the average interaction energy is $a\bar{g}=3.8\Omega_{\rm MF}$ [23], where the mean-field frequency [4] for our experimental parameters is $\Omega_{\rm MF}/2\pi \simeq 0.5$ Hz, i.e., $a\bar{g}/2\pi \simeq 1.9$ Hz.

The second term in Eq. (1) is an effective site-dependent Zeeman energy, arising from the quadratic spatial variation of the bias magnetic field along x, which produces a spin-dependent harmonic potential. As $\omega_r/\omega_x=27$, the corresponding effect on the transverse (y,z) motion is negligible, so that all atoms at site i have the same Zeeman energy. In Eq. (1), $\Omega(E_i) \equiv \Omega_i = \Omega' E_i + \Delta'$, where $\Omega' = -\delta \omega_x/\hbar \omega_x$, with $\delta \omega_x/2\pi=14.9$ mHz for our trap [4]. For atoms with the mean energy $\bar{E}_x \simeq k_B T_F/4$, $\Omega' \bar{E}_x/2\pi \simeq 2$ Hz. We define $\Delta' \equiv \Delta - \Omega' \bar{E}_x$, where Δ is the global detuning and $\Delta=0$ corresponds to $\Omega_i=0$ for the mean energy, $E_i=\bar{E}_x$.

A key feature of our experiments is the extraction of energy-resolved spin densities $n_{\uparrow_z,\downarrow_z}(E)$ by inverse-Abel transformation of the corresponding 1D spatial profiles $n_{\uparrow_z,\downarrow_z}(x)$, which are obtained from absorption images of a single cloud. The transform method requires a continuum approximation, which is justified for the x direction, where $k_B T_F/\hbar\omega_x=650$. Further, we require negligible energy space coherence; i.e., the atomic spins remain effectively localized in their individual energy sites. This assumption is justified by the very small transition matrix elements $< 10^{-4}\hbar\omega_x$ [24] between three-dimensional harmonic oscillator states, which arise from short-range interactions between two atoms [20].

In this regime, the spatial profile for each spin state $n_{\sigma}(x)$, $\sigma \equiv \uparrow_z, \downarrow_z$, is an Abel transform of the corresponding energy profile $n_{\sigma}(E)$ [20]:

$$n_{\sigma}(x) = \int dE |\phi_{E}(x)|^{2} n_{\sigma}(E)$$

$$= \frac{\omega_{x}}{\pi} \int_{0}^{\infty} dp_{x} n_{\sigma} \left(\frac{p_{x}^{2}}{2m} + \frac{m\omega_{x}^{2}}{2}x^{2}\right). \tag{2}$$

In Eq. (2), the last form is obtained by using a WKB approximation for the harmonic oscillator states $\phi_E(x)$ [20]. An inverse-Abel transform [20,25] of $n_{\sigma}(x)$ then determines $n_{\sigma}(E)$ with a resolution $\Delta E \simeq 0.04 E_F$ [20].

For the protocol of Fig. 1(a), discussed in detail below, Fig. 1(b) shows the measured *single-shot* spin density, $S_z(x,\phi) = [n_{\uparrow z}(x,\phi) - n_{\downarrow z}(x,\phi)]/2$, in units of the central total spin density n(0). Figure 1(c) shows the corresponding single-shot $S_z(E,\phi)$, obtained by inverse-Abel transformation of $S_z(x,\phi)$. We see that $S_z(E,\phi)$ appears smooth compared to the single-shot spin density $S_z(x,\phi)$, which requires averaging over several shots to obtain a smooth profile. To check that the inverse-Abel transform has adequate energy resolution, we Abel transform the extracted $S_z(E,\phi)$, yielding the red dotted curve of Fig. 1(b), which is consistent with the measured density profile [20].

Our experimental OTOC protocol, Fig. 1(a), applies a rotation ϕ to the total interacting spin system in between forward and time-reversed evolutions. Then, a measurement of s_{zi} is performed to diagnose the effects of the rotation on the spins at "site i" in energy space. We start by preparing a fully z-polarized state $|\downarrow_{z1}\downarrow_{z2}...\downarrow_{zN}\rangle \equiv |\psi_{z0}\rangle$ in a bias magnetic field $B_1 = 528.53$ G, where the scattering length $a_1 \equiv a = 4.24a_0$. Then we apply a 0.5 ms radiofrequency $(\pi/2)_y$ pulse (defined to be about the y axis), which is resonant with the $|\downarrow_z\rangle \rightarrow |\uparrow_z\rangle$ transition at the bias field B_1 , to produce an initial x-polarized N-atom state $|\psi_0\rangle = e^{-i(\pi/2)S_y}|\psi_{z0}\rangle = |\uparrow_{x1}\uparrow_{x2}...\uparrow_{xN}\rangle$. The system evolves for a time $\tau = 200$ ms at the initial bias magnetic field $B_1 = 528.53$ G. Then, a resonant radio-frequency pulse $(\phi)_x$, shifted in phase from the first pulse by $\pi/2$, rotates the N-atom state about the x axis [26] by a chosen angle ϕ . Immediately following this rotation, we

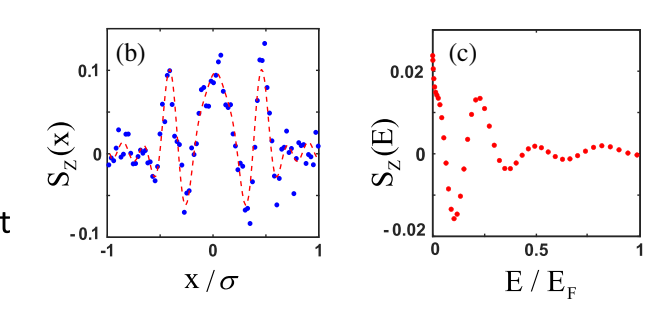


FIG. 1. Energy-resolved out-of-time-order correlation (OTOC) measurement. The system is initially prepared in a pure state, with the spins for atoms of energy $E_1, E_2, ..., E_N$ polarized along the -z axis. (a) OTOC sequence, after which the spatial profiles of the \uparrow_z and \downarrow_z states are measured for each cloud by resonant absorption imaging. (b) "Single-shot" spin density profile $S_z(x)$ (blue dots). For this measurement, the scattering length in the Hamiltonian H(a) is $a=4.24a_0$, $\phi=\pi$, and $\sigma=345~\mu\text{m}$. (c) An inverse-Abel transform of the spatial profile (blue dots) extracts the single-shot energy-resolved spin density $S_z(E)$ (red dots). An Abel transform of $S_z(E)$ yields the red dashed curve shown in (b), consistent with the data.

reverse the sign of the Hamiltonian by applying a $(\pi)_y$ pulse and tuning the bias magnetic field to a value $B_2 = 525.83$ G, where the scattering length $a_2 = -a$, i.e., $e^{i\pi S_y}H(-a)e^{-i\pi S_y} = -H(a)$, from Eq. (1). After the system evolves for an additional time τ , the bias field is ramped back to B_1 , and a final $(\pi/2)_y$ pulse is applied [20]. The final state of the N-atom system after the pulse sequence of Fig. 1(a) can be written as

$$|\psi_f\rangle = e^{-i(3\pi/2)S_y}W_{\phi}(\tau)|\psi_0\rangle,\tag{3}$$

where the W operator is defined by

$$W_{\phi}(\tau) = e^{iH(a)\tau} e^{-i\phi S_x} e^{-iH(a)\tau},\tag{4}$$

with $S_x = \sum_{i,\alpha_i} s_{x\alpha_i}$ the x component of the total spin vector for the N-atom sample and $|\psi_0\rangle$ the fully x-polarized state. After the pulse sequence, the spin densities $n_{\uparrow z}(x)$ and $n_{\downarrow z}(x)$ are measured for a single cloud using two resonant absorption images, separated in time by $10~\mu s$. We define one repetition of this experimental sequence as a "single shot," in Figs. 1(b) and 1(c). Inverse-Abel transformation of $[n_{\uparrow z}(x)-n_{\downarrow z}(x)]/2$ then measures $S_z(E_i,\phi)\equiv s_{zi}$, for a single shot, Fig. 1(c).

Now we connect the measured s_{zi} to information scrambling [10,13,19]. Consider a *single spin* labeled by α_i , with spin components $s_{x\alpha_i}$, $s_{y\alpha_i}$, $s_{z\alpha_i}$, interacting with the many-body system. It is straightforward to show [20]

$$C_{\alpha_i} \equiv \langle \psi_0 | [W_{\phi}(\tau), s_{x\alpha_i}] |^2 | \psi_0 \rangle = \frac{1}{2} - \langle \psi_f | s_{z\alpha_i} | \psi_f \rangle. \tag{5}$$

As the many-body operator W_{ϕ} and the single spin operator $s_{x\alpha_i}$ initially commute, i.e., $[W_{\phi}(0), s_{x\alpha_i}] = 0$, a measurement of $\langle \psi_f | s_{z\alpha_i} | \psi_f \rangle$ determines how two initially commuting operators fail to commute at a later time, providing a measure of scrambling.

In the experiments, we measure the *collective* spin operators $s_{zi} = \sum_{\alpha_i} s_{z\alpha_i}$, where $\alpha_i \equiv (n_i, n_y, n_z)$ for fixed

 n_i . The corresponding mean square commutator, averaged over the N_s spins with x energy E_i , is [20]

$$\frac{1}{N_s} \sum_{\alpha_i} C_{\alpha_i}(\phi, \tau) = \frac{1}{2} - \frac{1}{N_s} \sum_{\alpha_i} \langle \psi_f | s_{z\alpha_i} | \psi_f \rangle. \tag{6}$$

Further averaging Eq. (6) over atoms with energies within ΔE of $E_i \equiv E$, we replace the sum on the right-hand side by $S_z(E)\Delta E/[n(E)\Delta E]$, yielding the measured quantity

$$\mathcal{F}(E,\phi) \equiv \frac{1}{2} \frac{n_{\uparrow_z}(E,\phi) - n_{\downarrow_z}(E,\phi)}{n_{\uparrow_z}(E,\phi) + n_{\downarrow_z}(E,\phi)}.$$
 (7)

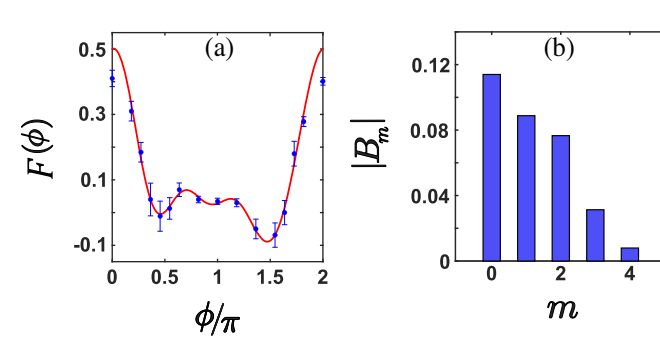
Here, $n(E) = n_{\uparrow_z}(E, \phi) + n_{\downarrow_z}(E, \phi)$ is independent of ϕ and $\mathcal{F}(E, 0) = 1/2$.

We can extract information about the many-body coherence from Eq. (6), by writing the sum on the right-hand side as $\sum_m e^{im\phi} B_m$ [20]. Nonvanishing coefficients B_m correspond to coherence between states for which the x component S_x of the total angular momentum differs by m [17,20]. Since the sum is real, $B_{-m} = B_m^*$, we can expand Eq. (7) for the measured, energy-selected average in the form

$$\mathcal{F}(E,\phi) = B_0 + \sum_{m>1} 2|B_m|\cos(m\phi + \varphi_m). \tag{8}$$

In fitting the data with Eq. (8), we restrict the range of m to 4. We find that the fits are not improved by further increase of m, consistent with the limited number of ϕ values measured in the experiments.

We measure spin density profiles $n_{\uparrow_z,\downarrow_z}(x,\phi)$ for a scattering length $a=4.24a_0$. The data are averaged over 6 repetitions for each ϕ , with the ϕ values chosen in random order. We begin by finding the *total* number of atoms in each spin state $N_{\uparrow_z,\downarrow_z}(\phi) = \int dx n_{\uparrow_z,\downarrow_z}(x,\phi)$ for the protocol of Fig. 1(a), to find the total collective spin projection S_z versus rotation angle ϕ , without energy restriction. Figure 2(a) shows the normalized S_z data $F(\phi) = \frac{1}{2}(N_{\uparrow_z} - N_{\downarrow_z})/(N_{\uparrow_z} + N_{\downarrow_z})$ (blue dots) and the fit of Eq. (8) (red



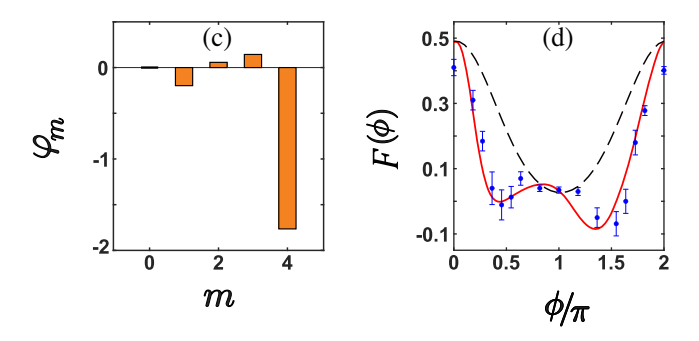


FIG. 2. Total collective spin projection S_z versus rotation angle ϕ without energy restriction. (a) $F(\phi) = \frac{1}{2}(N_{\uparrow_z} - N_{\downarrow_z})/(N_{\uparrow_z} + N_{\downarrow_z})$ (blue dots) for a measured scattering length $a_{\rm meas} = 4.24a_0$. The red solid curve is the fit of Eq. (8), which determines the magnitudes of the coherence coefficients $|B_m|$ (b) and corresponding phases φ_m (c). (d) Fit of the mean-field model of Ref. [4] to the data (blue dots) for a global detuning $\Delta=0$ with $a=a_{\rm meas}$ (black dashed curve) and with $a=2.63a_{\rm meas}$ (red solid curve).

curve), which determines the magnitude [Fig. 2(b)] and phase [Fig. 2(c)] of the average coherence coefficients B_m . We note that $F(0) \simeq F(2\pi) < 1/2$, the maximum for ideal conditions. This discrepancy arises from small variations in the phase shift of the final $\pi/2$ pulse, which is applied at a finite detuning as the magnetic field is ramped from B_2 back to its original value B_1 [20].

To check that the measurements are reasonable, we compare the ϕ -dependent data of Fig. 2 to a fit of our 1D mean-field model, which employs a calculated average transverse density \bar{n}_{\perp} to fit single-pulse spin-wave data with no free parameters [4]. The model, evaluated with a

global detuning $\Delta=0$, is shown in Fig. 2(d). To fit the observed ϕ dependence (red solid curve), the model requires a scattering length $a_{\rm eff}\equiv 2.63 a_{\rm meas}$, i.e., 2.63 times larger than the measured value $a_{\rm meas}=4.24a_0$, which yields the black dashed curve. The increased $a_{\rm eff}$ may occur because the measured coherence orders with |m|>1 arise from interactions, favoring the largest couplings in a manner that is not predicted by our model.

Figure 3 shows the energy-resolved measurements $\mathcal{F}(E,\phi)$, obtained by inverse-Abel transformation of the same data. The top row shows significant variation in symmetry and structure as the energy is varied from E=0

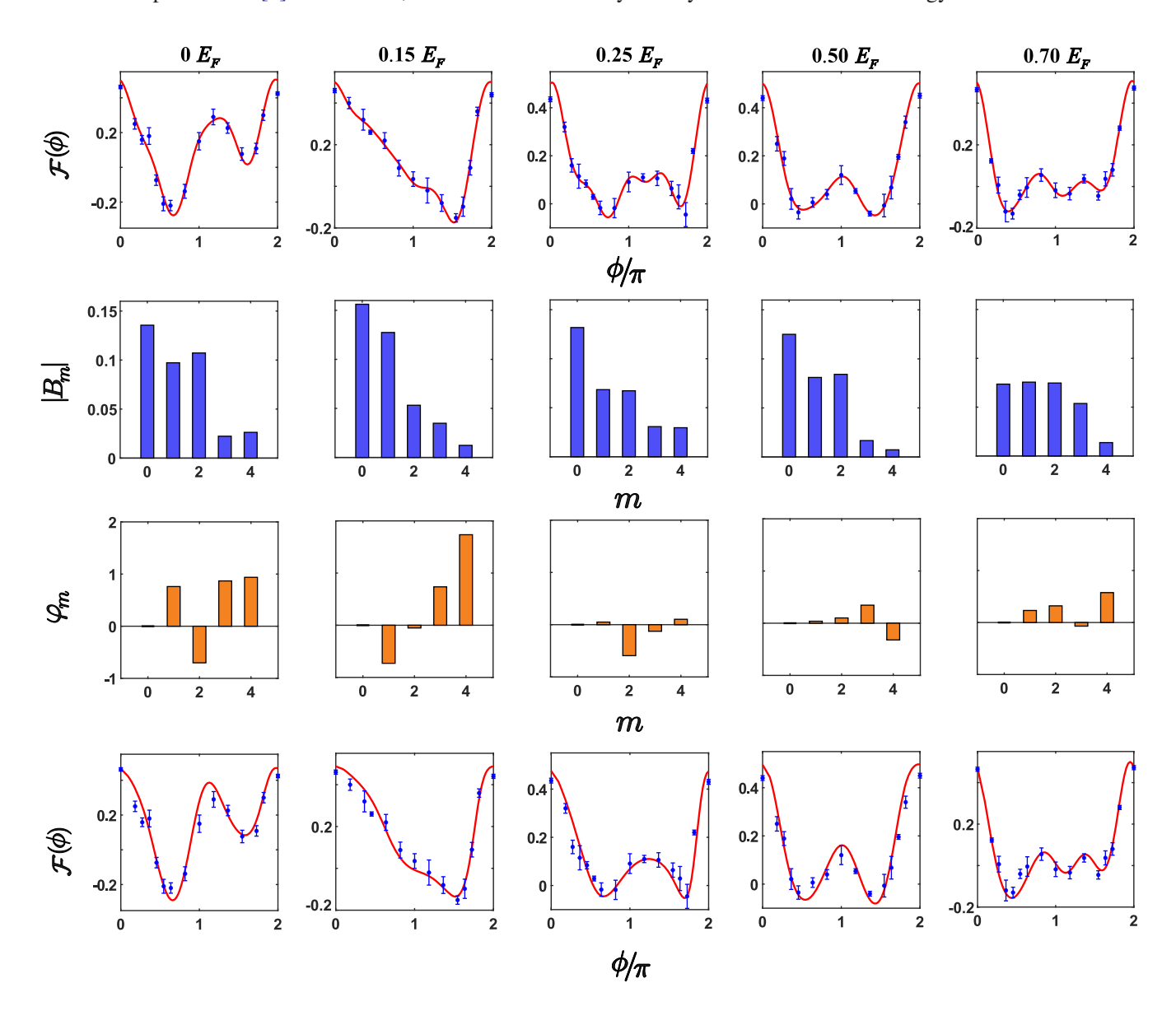


FIG. 3. Energy-resolved collective spin projection $S_z(E)$ versus rotation angle ϕ for spins of selected energies (left to right) $E/E_F=0$, 0.15, 0.25, 0.5, 0.7. Here, $\mathcal{F}(\phi)=\frac{1}{2}[n_{\uparrow}(E)-n_{\downarrow}(E)]/[n_{\uparrow}(E)+n_{\downarrow}(E)]$. The top row shows the data (blue dots) for a measured scattering length $a=4.24a_0$. The red solid curve is the fit of Eq. (8), which determines the magnitudes of the coherence coefficients $|B_m|$ (second row) and corresponding phases φ_m (third row). The bottom row shows the fits (red solid curves) of the mean-field model of Ref. [4] to the data (blue dots), using a scattering length 2.63 times the measured value and global detunings, ordered in energy, of $\Delta(\mathrm{Hz})=0$, 0.8, 0.65, -0.8, and 0.15.

to $E=0.7E_F$. The red solid curves in the first row show the fit of Eq. (8), which yields the magnitudes of the coherence coefficients $|B_m|$ and the corresponding phases φ_m . In the last row, we compare the data to fits of the mean-field model [4]. Again, the model captures the complex ϕ -dependent shapes of the data with $a_{\rm eff}=2.63a_{\rm meas}$, but a different detuning Δ is needed for each energy. This may be a consequence of averaging data over several detunings Δ , where each Δ rotates the direction of the ϕ -rotation axis by $\Delta \tau$ [26].

In summary, we have demonstrated a general method for measuring energy-resolved collective spin vectors in an energy-space lattice with effective long-range interactions. We have shown that an OTOC protocol can be implemented in this system and that many-body coherence can be measured in selected energy-space subsystems. Future measurement of time-dependent correlations between extensive subsets, $C_{ii}(t) \equiv \langle \psi_0 | s_{xi}(t) s_{xi}(t) | \psi_0 \rangle$ $\langle \psi_0 | s_{xi}(t) | \psi_0 \rangle \langle \psi_0 | s_{xj}(t) | \psi_0 \rangle$, enables a wide variety of protocols, extending correlation measurements in small numbers of trapped ions [27] to large quantum systems. For an initial x-polarized product state $|\psi_0\rangle$, $C_{ii}(t)=0$ for noninteracting systems and for our mean-field model, so that $C_{ij}(t) \neq 0$ signifies beyond mean-field physics. As $C_{ii}(0) = 0$, a scrambling time [28,29] is determined by observing the evolution from the product state to a correlated state.

Primary support for this research is provided by the Air Force Office of Scientific Research (FA9550-16-1-0378) and the National Science Foundation (PHY-2006234). Additional support for the JETlab atom cooling group has been provided by the Physics Division of the Army Research Office (W911NF-14-1-0628) and by the Division of Materials Science and Engineering, the Office of Basic Energy Sciences, Office of Science, U.S. Department of Energy (DE-SC0008646).

- *Corresponding author. jethoma7@ncsu.edu
- [1] X. Du, Y. Zhang, J. Petricka, and J. E. Thomas, Controlling Spin Current in a Trapped Fermi Gas, Phys. Rev. Lett. **103**, 010401 (2009).
- [2] S. Smale, P. He, B. A. Olsen, K. G. Jackson, H. Sharum, S. Trotzky, J. Marino, A. M. Rey, and J. H. Thywissen, Observation of a transition between dynamical phases in a quantum degenerate Fermi gas, Sci. Adv. 5, eaax1568 (2019).
- [3] X. Du, L. Luo, B. Clancy, and J. E. Thomas, Observation of Anomalous Spin Segregation in a Trapped Fermi Gas, Phys. Rev. Lett. 101, 150401 (2008).
- [4] S. Pegahan, J. Kangara, I. Arakelyan, and J. E. Thomas, Spin-energy correlation in degenerate weakly interacting Fermi gases, Phys. Rev. A 99, 063620 (2019).
- [5] F. Piéchon, J. N. Fuchs, and F. Laloë, Cumulative Identical Spin Rotation Effects in Collisionless Trapped Atomic Gases, Phys. Rev. Lett. 102, 215301 (2009).

- [6] S. S. Natu and E. J. Mueller, Anomalous spin segregation in a weakly interacting two-component Fermi gas, Phys. Rev. A 79, 051601 (2009).
- [7] C. Deutsch, F. Ramirez-Martinez, C. Lacroûte, F. Reinhard, T. Schneider, J. N. Fuchs, F. Piéchon, F. Laloë, J. Reichel, and P. Rosenbusch, Spin Self-Rephasing and Very Long Coherence Times in a Trapped Atomic Ensemble, Phys. Rev. Lett. 105, 020401 (2010).
- [8] A. P. Koller, M. L. Wall, J. Mundinger, and A. M. Rey, Dynamics of Interacting Fermions in Spin-Dependent Potentials, Phys. Rev. Lett. 117, 195302 (2016).
- [9] U. Ebling, A. Eckardt, and M. Lewenstein, Spin segregation via dynamically induced long-range interactions in a system of ultracold fermions, Phys. Rev. A **84**, 063607 (2011).
- [10] M. Gärttner, J. G. Bohnet, A. Safavi-Naini, M. L. Wall, J. J. Bollinger, and A. M. Rey, Measuring out-of-time-order correlations and multiple quantum spectra in a trappedion quantum magnet, Nat. Phys. 13, 781 (2017).
- [11] G. Bentsen, T. Hashizume, A. S. Buyskikh, E. J. Davis, A. J. Daley, S. S. Gubser, and M. Schleier-Smith, Treelike Interactions and Fast Scrambling with Cold Atoms, Phys. Rev. Lett. 123, 130601 (2019).
- [12] J. Eisert, M. Friesdorf, and C. Gogolin, Quantum manybody systems out of equilibrium, Nat. Phys. 11, 124 (2015).
- [13] M. Schleier-Smith, Probing information scrambling, Nat. Phys. 13, 724 (2017).
- [14] B. Swingle and N. Y. Yao, Seeing scrambled spins, Physics **10**, 82 (2017).
- [15] J. Li, R. Fan, H. Wang, B. Ye, B. Zeng, H. Zhai, X. Peng, and J. Du, Measuring Out-of-Time-Order Correlators on a Nuclear Magnetic Resonance Quantum Simulator, Phys. Rev. X 7, 031011 (2017).
- [16] J. Marino and A. M. Rey, Cavity-QED simulator of slow and fast scrambling, Phys. Rev. A **99**, 051803 (2019).
- [17] M. Gärttner, P. Hauke, and A. M. Rey, Relating Out-of-Time-Order Correlations to Entanglement via Multiple-Quantum Coherences, Phys. Rev. Lett. **120**, 040402 (2018).
- [18] J. Baum, M. Munowitz, A. N. Garroway, and A. Pines, Multiple-quantum dynamics in solid state NMR, J. Chem. Phys. 83, 2015 (1985).
- [19] R. J. Lewis-Swan, A. Safavi-Naini, J. J. Bollinger, and A. M. Rey, Unifying scrambling, thermalization and entanglement through measurement of fidelity out-of-time-order correlators in the Dicke model, Nat. Commun. 10, 5007 (2019).
- [20] See Supplemental Material at http://link.aps.org/supplemental/10.1103/PhysRevLett.126.070601 for a description of the experimental details and of the inverse Abel-transform method.
- [21] M. E. Gehm, S. L. Hemmer, K. M. O'Hara, and J. E. Thomas, Unitarity-limited elastic collision rate in a harmonically trapped Fermi gas, Phys. Rev. A **68**, 011603 (2003).
- [22] The number of atoms Δn_i at site i, i.e., in x mode E_i , summed over y, z transverse modes, is $\Delta n_i \simeq 3\Delta E_i N/E_F (1-E_i/E_F)^2$. With $\Delta E_i = \hbar \omega_x$, $N = 6.5 \times 10^4$, and $E_i = E_F/2$, we find $\Delta n_i \simeq 74$.
- [23] Here, we employ a continuum approximation with $\bar{g} \equiv \int dn P(n) \int dn' P(n') g(n, n')$, in the notation of Ref. [4].

- [24] Nonzero matrix elements arise for transitions between states of relative motion with even x quantum number 2n and azimuthal quantum number l=0 [20]. For our trap, $\sqrt{\hbar/m\omega_x} \simeq 8.5~\mu \text{m}$ and $\nu_r/\nu_x = 27$. With $a=4.24a_0$, $\langle 2n', m'_r|H'|2n, m_r\rangle/h\nu_x \simeq 3.2\times 10^{-4}/(n'n)^{1/4}$, independent of the radial quantum numbers m_r, m'_r .
- [25] G. Pretzier, A new method for numerical Abel-inversion, Z. Naturforsch. A 46, 639 (1991).
- [26] Note that a nonzero detuning Δ changes the effective axis of rotation to $\hat{e}_{x'} = \cos(\Delta \tau)\hat{e}_x + \sin(\Delta \tau)\hat{e}_y$ without changing the general ϕ -dependent structure of the OTOC [20].
- [27] P. Richerme, Z.-X. Gong, A. Lee, C. Senko, J. Smith, M. Foss-Feig, S. Michalakis, A. V. Gorshkov, and C. Monroe, Non-local propagation of correlations in quantum systems with long-range interactions, Nature (London) 511, 198 (2014).
- [28] A. Y. Guo, M. C. Tran, A. M. Childs, A. V. Gorshkov, and Z.-X. Gong, Signaling and scrambling with strongly long-range interactions, Phys. Rev. A **102**, 010401 (2020).
- [29] J. Maldacena, S. H. Shenker, and D. Stanford, A bound on chaos, J. High Energy Phys. 08 (2016) 106.